13 August 1999

ELSEVIER

Chemical Physics Letters 309 (1999) 157–164

CHEMICAL PHYSICS LETTERS

www.elsevier.nl/locate/cplett

Photodissociation of an alkyl nitrite at a liquid surface: flight-time distributions of NO and HNO

Alan Furlan *

Physikalisch-Chemisches Institut der Universität Zürich, Winterthurerstrasse 190, CH-8057 Zurich, Switzerland

Received 26 April 1999; in final form 15 June 1999

Abstract

The photochemistry at a gas–liquid interface was investigated by time-of-flight quadrupole mass spectroscopy. A liquid film of dodecyl dinitrite ($ONO(CH_2)_{12}ONO$), dissolved in squalane ($C_{30}H_{62}$), was irradiated with low-fluence laser pulses at 275 and 355 nm. The translational temperature of most NO and all HNO desorbate is in equilibrium with the liquid. A quantitative simulation requires that diffusion and radical reactions in the liquid are included. Ejection of hyperthermal NO ($T_{trans} = 500$–2200 K) was also observed. The results are compared to those of alkyl nitrite monomers, clusters and solid films. © 1999 Elsevier Science B.V. All rights reserved.

1. Introduction

Many important technological and environmental processes are initiated by photoabsorption of molecules at gas–liquid interfaces [1]. However, only few photochemical studies have focused on *liquid* surfaces. This is partly due to the limited number of molecular-level probe techniques and the technical difficulty of studying liquid surfaces under clean, high-vacuum conditions. A recently developed film preparation technique allows the study of clean liquid surfaces in high vacuum [2]. The technique involves the formation of a fresh, continuously renewed liquid film on a rotatable disk. We have adopted the film preparation method and combined it with time-of-flight quadrupole mass spectroscopy (TOF-QMS) to explore the photo-chemistry at gas–liquid interfaces.

In this work, the photoproducts desorbing from an alkyl nitrite/alkane solution are investigated. The choice of an alkyl nitrite is motivated by the large number of photodissociation studies on nitrites in different environments such as clusters, solid surfaces and matrices. The goal is to explore the characteristics of the photochemistry at a *gas–liquid* interface and compare the results with those found at solid surfaces and in clusters. Some recent photodissociation studies of alkyl nitrites in different environments are now briefly reviewed.

Under *single molecule* conditions in the gas phase, the primary photodissociation step of alkyl nitrites, RONO, is exclusively the decay to RO + NO (R = methyl, ethyl, isopropyl, and tert-butyl) [3,4]. At wavelengths below 300 nm, the molecules are excited to the highly repulsive S_2 state, followed by a fast, direct cleavage of the RO–NO bond. Absorption above 310 nm promotes RONO to the quasi-bound S_1 ($n\pi^*$) state which undergoes vibrational

---

* Fax: +41-1-635-6813; e-mail: furlan@pci.unizh.ch

PII: S0009-2614(99)00692-2

predissociation within ≈ 300 fs [4,5]. Even though the S_1 and S_2 decay mechanisms are different, a similar fraction of the excess energy is partitioned to fragment recoil (55% at 248 nm [3], 65% at 364 nm [6] for R = methyl). The kinetic energy of the fragment pairs decreases slightly with the size of R [3].

NO fragments ejected off RONO *clusters* (R = methyl, tert-butyl) exhibit a bimodal rotational distribution [7]. It was proposed that rotationally hot NO arises from cluster surface molecules, whereas cold NO originates from the cluster interior. Recently nitroxyl (HNO) and formaldehyde (H_2CO) were found as additional cluster products, besides NO + H_3CO [8].

Simpson et al. probed the translational and internal state distributions of NO ejected from a *solid film* of iso- and tert-butyl nitrite after irradiation at 351 nm [9]. A bimodal rotational distribution was observed. Jenniskens et al. measured TOF distributions of NO desorbed off a solid tert-butyl nitrite film (0.15–50 monolayers on Ag(111) after irradiation at 355 nm [10]). The spectra were fitted by the sum of a thermal and a hyperthermal Maxwellian distribution. From the dependence of the TOF profiles on the film thickness, the authors concluded that those molecules directly adsorbed on Ag yield thermalized NO. Intermediate layers give no NO contribution due to complete caging, while the topmost monolayer yields hyperthermal NO [10]. The excitation process at 266, 355 and 532 nm was found to be direct (without substrate mediation) [11]. Fieberg et al. found a dependence of the fast and slow signal contributions on the detection angle [12]. Photolysis of methyl nitrite in *cryogenic matrices* was shown to produce *exclusively* HNO and H_2CO by cage recombination of the initially formed NO + H_2CO [13,14].

The TOF measurements presented in this work were carried out with dodecyl-1,12-dinitrite, dissolved in squalane ($C_{30}H_{62}$). The chromophore consists of a long alkane chain with two terminal −ONO groups, as depicted in Fig. 1, along with the absorption spectrum of a solution in squalane. Squalane is transparent in this wavelength range and is expected to perturb the electronic states of the chromophore only very weakly. The absorption spectrum in Fig. 1 is almost identical with that of methyl nitrite. The similarity is attributed to a strong localization of the excitation on the –N=O part of the molecule. Similar decay paths for dodecyl dinitrite and methyl nitrite are therefore expected, in analogy to previous photodissociation results of different alkyl nitrites [3].

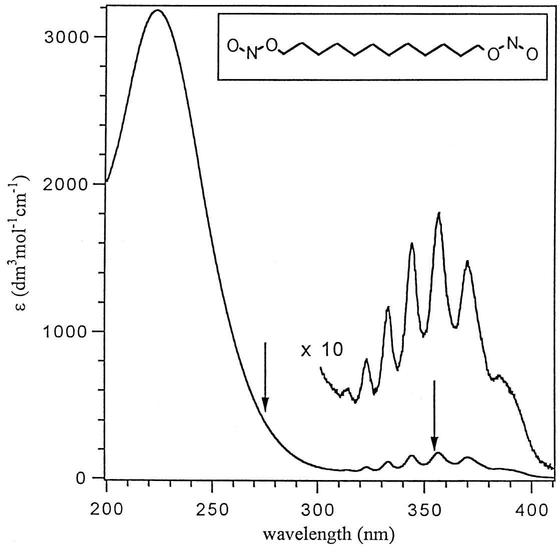

Fig. 1. Absorption spectrum of dodecyl dinitrite (inset) dissolved in squalane (2×10^{-6} M). The photolysis wavelengths used in this study are indicated by arrows.

2. Experimental

The technique used to prepare clean and continuously renewed liquid surfaces in vacuum has been described elsewhere [2,15]. Briefly, a rotating aluminum wheel was partially submersed in a reservoir filled with the liquid. The liquid layer on the wheel which rotated with a speed of 0.3 Hz was scraped to a thickness of 100 ± 30 μm.

Dodecyl dinitrite was synthesized from dodecanediol according to a published procedure [16] and purified by vacuum distillation. Solutions of dodecyl dinitrite in squalane (99%, Aldrich) were prepared at concentrations of 2×10^{-6} and 2×10^{-7} mol l^{-1}. The concentrations were determined spectrophotometrically. The extinction coefficient ε of dodecyl dinitrite is 385 dm^3 mol^{-1} cm^{-1} at 275 nm, and 160 dm^3 mol^{-1} cm^{-1} at 355 nm. The liquid was cooled to 2°C by Peltier elements. The pressure in the source chamber which is pumped by two diffusion pumps and a liquid nitrogen-cooled trap was $\approx 5 \times 10^{-6}$ mbar. The detector was contained in a bakeable ultrahigh vacuum system [17]. After a total flight distance of 374 mm, the molecules were ionized by electron impact and mass filtered in a QMS.

Excitation laser pulses at 275 nm and pulse energies of 1–20 mJ/pulse were obtained by frequency-doubling the output of a Nd:YAG-pumped dye laser. The third harmonic of the Nd:YAG laser was used for photolysis at 355 nm. A small central part of the beam was selected to obtain a uniform intensity profile.

The collimated laser beam was weakly focused in one direction with a 700 mm cylindrical lens, and directed onto the liquid surface at a grazing angle of 87°. Taking reflexion losses into account, a laser fluence of the beam refracted into the liquid of 2–40 mJ cm^{-2} was obtained at 275 nm and 5–100 mJ cm^{-2} at 355 nm. The beam reflected off the Al disk was directed out of the chamber via a dichroic mirror. The accumulation of surface contaminations was checked tensiometrically after each measurement [18].

3. Results

Following irradiation of the dodecyl dinitrite/squalane film at 275 and 355 nm, a signal was observed exclusively at the masses of NO ($m/e = 30$) and HNO ($m/e = 31$). The TOF spectra shown in Fig. 2 were recorded with a dodecyl dinitrite concentration of 2×10^{-6} mol l^{-1} and laser fluences of 18 and 60 mJ cm^{-2} at 275 and 355 nm, respectively. The TOF measurements at 275 nm were also carried out with a 2×10^{-7} mol l^{-1} solution. The higher dilution did not affect the shape of the TOF profiles shown in Fig. 2 but resulted in a signal reduction approximately proportional to the dilution factor. The spectra changed dramatically, however, if the chromophore exceeded the saturation concentration of $\approx 8 \times 10^{-6}$ mol l^{-1} at 2°C. The TOF profiles shifted to shorter flight times typical for ablation [15,19], and bursts of signal were observed at irregular time intervals and at a large number of masses. These bursts are attributed to the irradiation of dodecyl dinitrite grains precipitated at the surface of the saturated liquid.

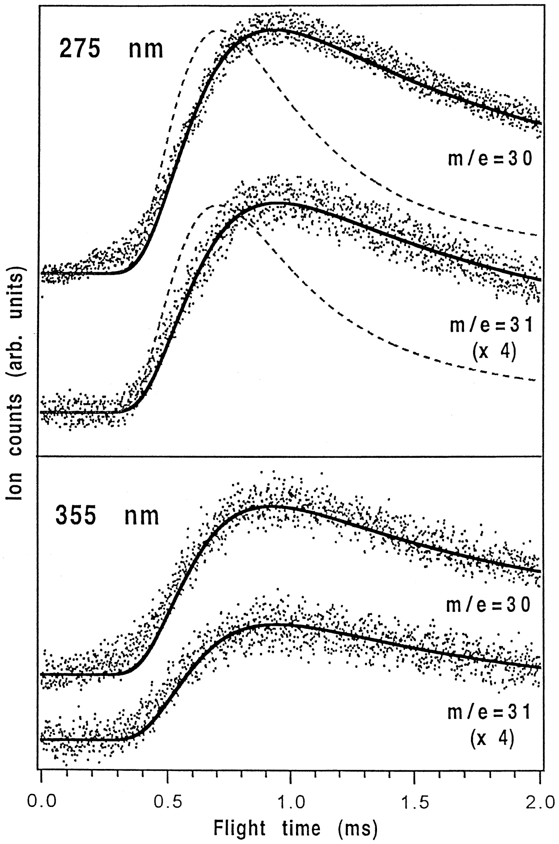

Fig. 2. TOF distributions of NO$^+$ ($m/e = 30$) and HNO$^+$ ($m/e = 31$) following irradiation of dodecyl dinitrite (2×10^{-6} M) dissolved in squalane at 275 and 355 nm. The dashed lines represent flight time distributions for prompt desorption of NO and HNO from the topmost liquid layer with $T_{\text{trans}} = 275$ K. The solid lines were calculated by including bulk diffusion and radical reactions.

Following excitation at 275 nm, a ratio of the TOF signals NO$^+$/HNO$^+$ of 4.0 ± 0.4 was found, while at 355 nm the ratio was slightly larger (5.5 ± 0.6). The fraction of HNO$^+$ which is cracked to NO$^+$ in the ionizer is estimated to be 30–50%, based on cracking ratios of related compounds under the same experimental conditions. This yields a true NO/HNO ratio of ≈ 2–3 at 275 nm, and a slightly higher ratio at 355 nm.

The intensities of the $m/e = 30$ and $m/e = 31$ signals were found to increase linearly with fluence (in the range 2–40 mJ cm^{-2} at 275 nm, and 5–100 mJ cm^{-2} at 355 nm), while the shapes of the profiles remained unaffected. This indicates that heating of the irradiated liquid volume is negligible in this range of fluences. The temperature rise ΔT can be estimated using the following expression which assumes full conversion of the photon energy into heat and no cooling by the surrounding liquid within the irradiation time

$$\Delta T = \frac{\Delta E}{c_{\mathrm{v}} V} = \frac{\Delta E \varepsilon c}{0.43 c_{\mathrm{v}} A}, \qquad (1)$$

where ΔE is the fraction of the pulse energy entering the liquid, c_{v} is the heat capacity of squalane (1.5 J K^{-1} cm^{-3}), and V is the liquid volume absorbing $1/e$ of the pulse energy. The volume is calculated from the irradiated surface area A, the extinction coefficient ε and the concentration c of dodecyl dinitrite. Due to the low concentration, the liquid film is nearly transparent (penetration depth $0.43/\varepsilon c \approx 5$ m). At a pulse energy of 10 mJ at 275 nm, Eq. (1) yields $\Delta T \approx 1 \times 10^{-3}$ K. This confirms that under these experimental conditions the process can be regarded as isothermal.

The TOF profiles measured at $m/e = 30$ and $m/e = 31$ have similar shapes at both wavelengths, particularly in the fall-off region > 1 ms (Fig. 2). The onset of the $m/e = 30$ signal, however, occurs at a shorter flight time than the $m/e = 31$ signal and exhibits a small shoulder between 0.2 and 0.4 ms. The shoulder appears at both excitation wavelengths. The signal-to-noise ratio of the spectra recorded at 275 nm was substantially better than at 355 nm, even though a higher laser fluence and longer averaging (80 000 shots) was used to record the latter. A further increase of the laser fluence at 355 nm was avoided because of multiphoton processes. The following discussion refers to the measurements at 275 nm, and the results at 355 nm are only specified to point out deviations from the 275 nm data.

4. Discussion

In general, the signal decay at *long* flight times is a signature of species originating from deeper liquid layers [15]. The late arrival times of these species at the detector are due to diffusion to the surface, followed by delayed desorption [15,20]. On the other hand, the signal *onset* reflects the degree of thermalization of the nascent fragments before they leave the surface.

As a first approach for fitting the TOF profiles, it is assumed that the species NO and HNO ejected from the liquid surface are thermally equilibrated with the surrounding solvent. Furthermore only the excited chromophores located in the topmost liquid layer are allowed to contribute to desorption. For this simplest case the flight time distribution $P(t)$ measured with a density-sensitive detector can be expressed by a Maxwellian distribution [21]

$$P(t) = \frac{N}{t^4} \exp\left[- \frac{md^2}{2kTt^2} \right], \qquad (2)$$

where N is a normalization constant, m and T are the mass and temperature of the desorbed molecules, and d is the surface–ionizer distance. The dashed lines in Fig. 2 correspond to Maxwellian distributions obtained with $T = 275$ K. The poor agreement between these curves and the measured data, particularly at long flight times, clearly shows that NO and HNO formed in deeper layers of the liquid also contribute to the desorption flux.

The agreement with the measured spectra strongly improves if bulk contributions to the signal are included in the calculation. The solid lines shown in Fig. 2 were computed by numerical integration of one-dimensional coupled differential equations, which govern the diffusion and surface evaporation of NO and HNO, and bulk recombination kinetics. Details of the calculation have been described elsewhere [15], and only the specific reaction scheme used for this system is presented here.

Absorption of laser light by dodecyl dinitrite molecules is followed by dissociation of the excited species to radical pairs RO + NO at the surface and within the liquid,

$$\mathrm{RONO} + h\nu \rightarrow \mathrm{RO} + \mathrm{NO}, \qquad (3)$$

where RO = $\mathrm{ONO(CH_2)_{12}O}$. If the excited molecules are located in the surface layer and are oriented with the –ONO groups pointing away from the liquid, then the NO fragments can be directly ejected into the gas phase.

$$\mathrm{RO} + \mathrm{NO(surface)} \rightarrow \mathrm{RO} + \mathrm{NO(ejected)}\,. \qquad (4)$$

Directly ejected NO fragments are expected to have a highly hyperthermal velocity distribution similar to the fragments in gas-phase photodissociation. Fragment pairs RO + NO formed in deeper layers of the liquid are surrounded by cages of squalane molecules. These fragment pairs can recombine geminately (5), disproportionate to HNO and R′O (with $\mathrm{R}' = \mathrm{ONO(CH_2)_{11}CHO}$) (6), or escape from the cage (7),

$$\{\mathrm{RO} + \mathrm{NO}\} \rightarrow \mathrm{RONO}\,, \qquad (5)$$

$$\{\mathrm{RO} + \mathrm{NO}\} \rightarrow \mathrm{R'O} + \mathrm{HNO}\,, \qquad (6)$$

$$\{\mathrm{RO} + \mathrm{NO}\} \rightarrow \mathrm{RO(free)} + \mathrm{NO(free)}\,. \qquad (7)$$

The parentheses indicate the liquid cage surrounding the geminate pair. The mobile radicals (7) diffuse freely in solution and undergo the combination reactions (8) and (9),

$$\mathrm{RO} + \mathrm{NO} \rightarrow \mathrm{RONO}\,, \qquad (8)$$

$$\mathrm{RO} + \mathrm{RO} \rightarrow \mathrm{ROOR}\,. \qquad (9)$$

The exothermic and presumably barrierless radical reactions (8) and (9) ($\Delta H \approx -175$ and -150 kJ $\mathrm{mol^{-1}}$, respectively) [22,23] are modeled with diffusion-limited rates [15,24]. Disproportionation of the *free* radicals was also considered as a potential source of HNO,

$$\mathrm{RO} + \mathrm{NO} \rightarrow \mathrm{R'O} + \mathrm{HNO}\,. \qquad (10)$$

Although reaction (10) is exothermic (-105 kJ $\mathrm{mol^{-1}}$) [7], it may be kinetically hindered for thermalized radicals. The calculated temporal profiles of HNO formed promptly inside the cage (6) and by encounters of free radicals (10) are somewhat different and could in principle be distinguished experimentally. However, under our conditions the HNO source given by Eq. (10) is negligible even if one assumes the highest possible (diffusion-limited) rate, since the concentration of free radicals generated by a laser pulse is very low.

The diffusion constant of NO and HNO in squalane at 275 K was estimated to be 1×10^{-7} $\mathrm{cm^2\,s^{-1}}$, based on the measured viscosity of squalane (90 cP) and scaling with published values of a related solute/solvent system [25]. After diffusion to the surface, the NO and HNO molecules evaporate with a diffusion-limited rate [15].

The solid lines in Fig. 2 were calculated with the kinetic scheme given by Eqs. (5)–(10), while the direct (hyperthermal) desorption (Eq. (4)) was neglected. The agreement with both the measured NO and HNO spectra is quantitative except for the onset of the NO spectrum which is described later. The ratio of the calculated yields of NO and HNO was adjusted to the measured ratio of ≈ 2 by setting the cage escape probability to 2% (based on literature values for liquids of similar viscosity [15,26]) and the probability for HNO formation to 1%.

As noted above, the simulated profiles of NO fragments in Fig. 2 fail to reproduce the shoulder at the onset of the measured NO spectra around 120 μs. Fig. 3 shows the difference spectra obtained by subtracting the best-fit isothermal simulations (solid lines in Fig. 2) from the TOF profiles of $\mathrm{NO^+}$ and $\mathrm{HNO^+}$. The difference spectrum of NO (Fig. 3a) has a clear hyperthermal contribution whereas the difference spectrum of HNO shows only a weak deviation from the baseline at flight times > 400 μs. This deviation depends critically on the relative scaling of the measured and the calculated spectra. The signal-to-noise ratio at $m/e = 31$ is insufficient for a detailed analysis. As a preliminary result it is clear, however, that the hyperthermal HNO contribution is very small, with a fraction of $< 0.5\%$ relative to the thermal HNO signal.

The calculated TOF profiles shown in Fig. 3c represent Maxwellian distributions with $T_{\mathrm{trans}} = 1000$ and 2000 K, respectively, assuming prompt NO desorption. The fit of the hyperthermal NO signal (Fig. 3a) with a single Maxwellian distribution is not satisfactory. The forward convolution technique was therefore used to calculate a flight time distribution $P(t)$ from a single kinetic energy distribution $P(E_{\mathrm{T}})$ of arbitrary shape, as is common in gas-phase photodissociation studies [27]. The best-fit $P(t)$, shown by the solid line in Fig. 3a, was obtained by forward convolution of the $P(E_{\mathrm{T}})$ displayed in Fig. 4. At high kinetic energies, the $P(E_{\mathrm{T}})$ follows the shape of a Maxwellian distribution at ≈ 2200 K ($\sim \sqrt{E_T} \times \exp(-E_{\mathrm{T}}/kT)$), while at low energies it smoothly approaches a ≈ 500 K curve. The average kinetic energy $\langle E_{\mathrm{T}} \rangle \approx 23$ kJ $\mathrm{mol^{-1}}$ corresponds to a 'tem-

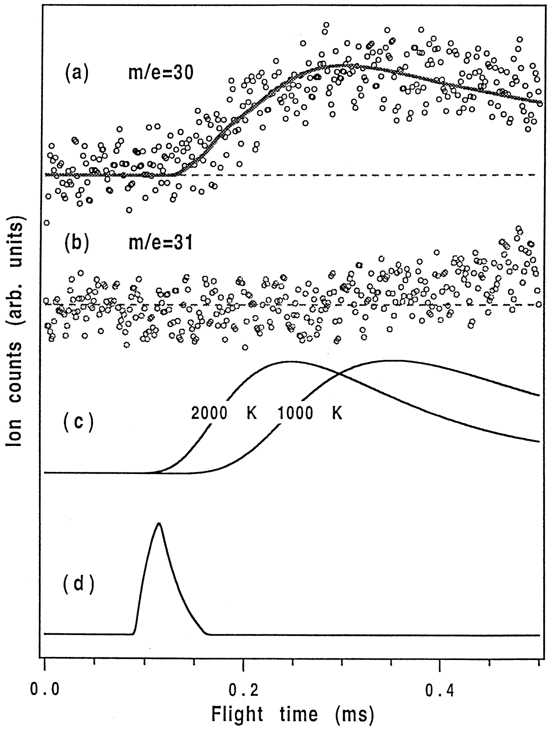

Fig. 3. Difference spectra of (a) $m/e = 30$ and (b) $m/e = 31$ obtained by subtracting the best-fit simulated TOF profiles for *isothermal* desorption ($T = 275$ K) from the measured spectra of Eq. (1). The solid line in trace (a) represents the forward-convolution of the kinetic energy distribution shown in Fig. 4. (c) Calculated TOF profiles of NO assuming prompt desorption with a Maxwellian distributions corresponding to $T = 1000$ and $T = 2000$ K. (d) Calculated TOF profile for gas-phase photodissociation of isolated RONO molecules obtained by forward-convolution of the $P(E_T)$ displayed by the dashed line in Fig. 4.

perature' $\langle E_T \rangle / 2k \approx 1370$ K. Details of the analysis will be presented elsewhere [28].

Fig. 3d represents the calculated TOF profile expected for the *gas-phase* photodissociation of isolated RONO molecules. This profile was obtained by forward-convolution of an adapted kinetic energy distribution [1] for the gas-phase photodissociation of *t*-butyl nitrite [3]. Fig. 4 illustrates that the highest kinetic energy of NO from the *liquid* is approximately equal to the average kinetic energy of *gas-phase* NO fragments. The fastest NO ejected off the liquid must originate from surface layer molecules with a nitrite group pointing toward the gas phase, allowing NO the ejection of fragments without intermediate collisions. However, only a small fraction of the NO from the liquid reaches the high kinetic energies typical for the gas-phase distribution. This could indicate that only few RONO molecules at the surface are oriented with the –ONO group pointing out of the liquid. Most NO fragments undergo at least one collision with neighboring molecules before leaving the liquid.

The TOF spectra in Fig. 2 and those of solid alkyl nitrite films adsorbed on *solid* surfaces exhibit several marked differences [10,12]. In contrast to the present study, no HNO was found after irradiation of solid *t*-butyl nitrite [10] and methyl nitrite [12] adsorbed on Ag(111). For *t*-butyl nitrite this is not surprising since the disproportionation reaction (6) cannot occur due to the lack of an alpha-hydrogen

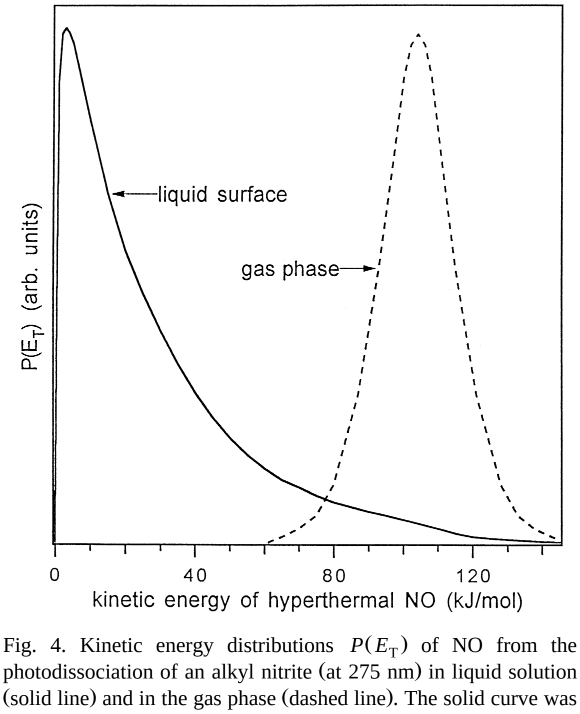

Fig. 4. Kinetic energy distributions $P(E_T)$ of NO from the photodissociation of an alkyl nitrite (at 275 nm) in liquid solution (solid line) and in the gas phase (dashed line). The solid curve was obtained by fitting the fast signal contribution of the NO spectrum shown in Fig. 2a. The gas phase curve was calculated by adapting a previously published $P(E_T)$ [3].

---

[1] The RO counterfragment mass was set to infinity. In the gas phase a fraction of 40% of the available energy was assumed to be channeled into fragment recoil.

atom. But, even for unbranched alkyl nitrites [12], the yield of HNO from a *solid* film is expected to be much lower than the yield from a liquid film, since HNO is mainly formed in the bulk by the cage-mediated reaction (6) which requires full solvation of the geminate pairs RO + NO. Due to the very low diffusion coefficient in the cold solid film, the fraction of HNO molecules which reach the gas–solid interface and desorb within the timescale of the experiment is much smaller than in the liquid film. Typical diffusion constants of solids are 10^{-12}–10^{-10} cm^2 s^{-1}, about four orders of magnitude smaller than in the liquid [29]. It may seem surprising, according to this argument, that HNO was also found as a photodissociation product ejected from supersonically cooled, *solid* methyl nitrite clusters [8]. The 'heat bath' represented by a cluster is so small, however, that the available energy deposited by a photon ($\approx 22\,000$ cm^{-1}) can be sufficient for evaporating the whole cluster. Thereby all photoproducts are released [8].

Another discrepancy between the solid and liquid surfaces are the disparate ratios of hyperthermal and thermal signal contributions. Jenniskens et al. found hyperthermal-to-thermal ratios ranging from ≈ 1 for low coverages ($\leqslant 1$ monolayer) to ≈ 8 at higher coverages [10]. The relative yield of *thermal* NO ejected off the liquid is roughly two orders of magnitude *larger* than in the solid film. This discrepancy is attributed to stronger caging and a lower diffusion coefficient in the bulk solid as compared to the liquid. A recent calculational study of solid and liquid matrices reported a dramatic drop of the cage escape probability as the matrix freezes [30]. The low diffusivity prevents NO molecules formed deep inside the film from reaching the surface within the timescale of the experiment. Finally, the desorption barrier for the thermalized NO may also be rate-limiting at the low temperature of the solid photodissociation experiments.

For a rough estimate of the relative yields of thermal and hyperthermal NO, the simulated liquid film is divided into a surface layer of variable thickness, and the bulk liquid. In the surface layer all NO fragments are assumed to be ejected promptly (within the first 1 μs timestep) according to Eq. (4), with $T_{\mathrm{trans}} = 2000$ K, while the NO fragments formed below this layer are treated with the isothermal model including the bulk reactions (5)–(10), diffusion and a desorption temperature $T = 275$ K. The best fit to the measured NO spectra was obtained with a surface layer thickness of 0.2 nm. All dodecyl dinitrite molecules which have an excited –ONO unit located within 0.2 nm from the gas-liquid interface, will eject hyperthermal NO. This highly simplified model assumes a step function in the cage escape probability (from 0.02 in the bulk to 1 in the surface layer). The desorption temperature and the number density in the interfacial region are also assumed to change abruptly. Since a single temperature fit cannot reproduce the hyperthermal contribution of the NO spectrum shown in Fig. 3, while a similar fit was successful for solid films, it is concluded that at the gas–liquid interface the transition between uncaged molecules and fully caged molecules is smoother than at a gas–solid interface. An improved calculation would require a more realistic modeling of caging, density and temperature profiles at the gas–liquid interface. Once these effects are correctly modeled one could use the fitted calculation to extract average orientations of the excited surface molecules. Refined calculations along this line are under way [28].

In summary, NO and HNO were the only photoproducts desorbing from a liquid solution of dodecyl dinitrite in squalane after irradiation at 275 and 355 nm. At both excitation wavelengths, approximately the same relative yield was found (NO/HNO ≈ 2–4). All HNO and most NO molecules desorb with a translational temperature in equilibrium with the surrounding solvent, indicating several collisions prior to desorption. A small fraction of the NO fragments desorb with high kinetic energies corresponding to temperatures in the range 500–2200 K. In contrast, in the photolysis at solid surfaces, the relative yield of thermalized NO desorbing from the liquid film is much larger than that from solid surfaces. This may reflect the weaker cage effect and larger diffusivity in the topmost layers of the liquid.

Acknowledgements

This work was supported by the Swiss National Foundation. The author thanks Professor J.R. Huber for his generous support.

References

[1] N.J. Turro (Ed.), Modern Molecular Photochemistry, University Science Books, Mill Valley, 1991.
[2] M.E. Saecker, G.M. Nathanson, J. Chem. Phys. 99 (1993) 7056.
[3] C.S. Effenhauser, P. Felder, J.R. Huber, J. Phys. Chem. 94 (1990) 296.
[4] A. Untch, R. Schinke, R. Cotting, J.R. Huber, J. Chem. Phys. 99 (1993) 9553.
[5] J.M. Mesdagh et al., J. Chem. Phys. 103 (1995) 1013.
[6] U. Brühlmann, M. Dubs, J.R. Huber, J. Chem. Phys. 86 (1987) 1249.
[7] E. Kades, M. Rösslein, J.R. Huber, J. Phys. Chem. 98 (1994) 13556.
[8] K. Bergmann, J.R. Huber, J. Phys. Chem. A 101 (1997) 259.
[9] C.J. Simpson, P.T. Griffiths, M. Towrie, Chem. Phys. Lett. 234 (1995) 203.
[10] H.G. Jenniskens, L. Philippe, W.v. Essenberg, M. Kadodwala, A.W. Kleyn, J. Chem. Phys. 108 (1998) 1688.
[11] H.G. Jenniskens, L. Philippe, M. Kadodwala, A.W. Kleyn, J. Phys. Chem. B 102 (1998) 8736.
[12] J.E. Fieberg, G.J. Szulczewski, J.M. White, Chem. Phys. Lett. 290 (1998) 268.
[13] R.P. Müller, P. Russegger, J.R. Huber, Chem. Phys. 70 (1982) 281.
[14] M.E. Jacox, F.L. Rook, J. Phys. Chem. 86 (1982) 2899.
[15] A. Furlan, G.E. Hall, J. Chem. Phys. 109 (1998) 10390.
[16] A.H. Blatt (Ed.), Organic Syntheses, Wiley, New York, vol. 2, 1943, p. 204.
[17] P. Felder, Chem. Phys. 143 (1990) 141.
[18] G.L. Gaines, Insoluble Monolayers at the Liquid Gas Interface, Wiley, New York, 1966.
[19] A. Furlan, Chem. Phys. Lett. 275 (1997) 239.
[20] A. Furlan, J. Phys. Chem. B 103 (1999) 1550.
[21] F.M. Zimmermann, W. Ho, Surf. Sci. Rep. 22 (1995) 127.
[22] L. Batt, K. Christie, R.T. Milne, A.J. Summers, Int. J. Chem. Kinet. 6 (1974) 877.
[23] P.H. Pine, J.B. Hendrickson, D.J. Cram, G.S. Hammond, Organic Chemistry, McGraw–Hill, Tokyo, 1980.
[24] P.W. Atkins, Physical Chemistry, Oxford University Press, Oxford, 1998.
[25] B.A. Kowert, N.C. Dang, J. Phys. Chem. A 103 (1998) 779.
[26] D. Booth, R.M. Noyes, J. Am. Chem. Soc. 82 (1960) 1868.
[27] R.K. Sparks, K. Shobatake, L.R. Carlson, Y.T. Lee, Chem. Phys. 75 (1981) 3838.
[28] A. Furlan, to be published.
[29] E.L. Cussler, Diffusion, Cambridge University Press, Cambridge, 1984.
[30] A.I. Krylov, R.B. Gerber, J. Chem. Phys. 100 (1994) 4242.